Physics-informed LSTMs improve streamflow prediction when storage-discharge dynamics are temporally resolved

Alberto Ardid[1,*], David Dempsey[1], Céline Cattoën[2,3], Markus Pahlow[1]

[1] Department of Civil and Environmental Engineering, University of Canterbury, Christchurch, New Zealand
[2] Earth Sciences New Zealand, Christchurch, New Zealand
[3] Te Pūnaha Matatini, University of Auckland, Auckland, New Zealand

Author email addresses

Alberto Ardid: alberto.ardid@canterbury.ac.nz
David Dempsey: david.dempsey@canterbury.ac.nz
Céline Cattoën: celine.cattoengilbert@earthsciences.nz
Markus Pahlow: markus.pahlow@canterbury.ac.nz

Preprint status

This manuscript is a non-peer-reviewed preprint submitted to EarthArXiv. The manuscript has also been submitted to Water Resources Research for peer review.

Corresponding author: Alberto Ardid (alberto.ardid@canterbury.ac.nz)

Physics-informed LSTMs improve streamflow prediction when storage–discharge dynamics are temporally resolved

Alberto Ardid[1,*], David Dempsey[1], Céline Cattoën[2,3], Markus Pahlow[1]

[1]University of Canterbury, Christchurch, New Zealand; [2]Earth Science New Zealand, Christchurch, New Zealand; [3]Te Pūnaha Matatini, University of Auckland, Auckland, New Zealand

*Corresponding author: Alberto Ardid (alberto.ardid@canterbury.ac.nz). ORCID: 0000-0001-8040-8193.

Keywords: streamflow prediction; physics-informed machine learning; LSTM; flood forecasting; hydrology

Key Points

- Adding a storage-discharge physics constraint to a neural network model improves hourly flood prediction in most catchments tested
- The improvement all but disappears at daily resolution, showing physics constraints only help when they match the data timestep
- The constraint yields interpretable recession timescales, showing the model learns physically plausible catchment storage behaviour

Abstract

Flood prediction at sub-daily resolution requires models that are accurate and physically plausible beyond observed conditions. We augment a per-basin Long Short-Term Memory network with a linear reservoir constraint (Q = KS), embedding storage-discharge dynamics as a soft physics loss, and evaluate it in hourly and daily streamflow-prediction experiments across New Zealand and Great Britain. At hourly resolution, the physics-informed LSTM improves performance in 99% and 91% of catchments, respectively, increasing median NSE from 0.30 to 0.44 in New Zealand and from 0.61 to 0.70 in Great Britain while learning physically plausible recession timescales. The largest gains occur where test-period flood recessions differ most from training conditions, indicating that the constraint is particularly useful for hydrological behaviour that is weakly represented during training. However, these benefits largely disappear at daily resolution, with improvements observed in only 14% and 21% of catchments in New Zealand and Great Britain, respectively. At hourly resolution, recession limbs span multiple timesteps and directly inform the storage–discharge constraint, which learns physically plausible effective recession timescales (median ~11.5 hours in New Zealand) that vary among catchments independently of catchment size; daily aggregation compresses these dynamics and substantially weakens that information. These results show that the value of physics-informed learning depends on whether the constrained physical process is resolved at the modelling timestep, and suggest that temporal resolution should be considered explicitly when designing and evaluating physics-informed hydrological models.

Introduction

Accurate streamflow prediction remains a central challenge in hydrology because catchment responses emerge from complex interactions among climate, topography, geology, and antecedent conditions. Recent advances in deep learning have substantially improved rainfall–runoff modelling, with Long Short-Term Memory (LSTM) networks demonstrating strong predictive skill across large and diverse catchment samples (Kratzert et al., 2018; Kratzert et al., 2019b; Lees et al., 2021) and matched or exceeded operational systems globally (Mai et al., 2022; Nearing et al., 2024). The consistent finding is that regional LSTMs leverage cross-catchment information in ways that calibrated process models cannot (Kratzert et al., 2019a). Similar results have been reported across continents (Mai et al., 2022) and at global scale (Nearing et al., 2024).

Despite this accomplishment, purely data-driven LSTMs offer no explicit physical learnings. Although they have been shown to remain accurate even for extreme events withheld from training (Frame et al., 2022) they are not constrained to respect mass balance or storage-discharge dynamics, and their behaviour under hydrological conditions not represented in the training data (out-of-distribution conditions) remains debated (Nearing et al., 2021). These considerations have motivated a growing body of work on physics-informed deep learning for hydrology. Differentiable parameter learning applied to the HBV conceptual hydrological model (Feng et al., 2022) demonstrated that embedding a conceptual model skeleton within a neural network yields comparable skill to unconstrained LSTMs while producing interpretable state variables, with advantages in climate-change extrapolation (Feng et al., 2023). Mass-conserving LSTMs (MC-LSTM) (Hoedt et al., 2021) enforce strict mass conservation through architectural constraints. However, recent work suggests that hard physical constraints can introduce trade-offs between physical consistency and predictive skill, motivating softer forms of physics regularisation (Frame et al., 2023). Neural ordinary differential equation (ODE) approaches (Höge et al., 2022) and hybrid HBV-LSTM architectures (Acuña Espinoza et al., 2024; Acuña Espinoza et al., 2025) occupy intermediate positions on the constraint-flexibility spectrum. Comprehensive reviews (Karniadakis et al., 2021; Shen et al., 2023; Willard et al., 2022) highlight growing evidence that physics-guided machine learning can improve physical consistency and out-of-sample generalisation relative to purely data-driven approaches.

An important insight from the interpretability literature is that unconstrained LSTMs can learn physically meaningful internal representations. For example, soil moisture and snow depth can be recovered from the cell states of an LSTM trained only on streamflow across CAMELS-GB catchments (Lees et al., 2022). The LSTM cell-state update is also mathematically analogous to a discretised linear reservoir (De la Fuente et al., 2024), with the forget gate controlling the persistence of stored information. This suggests that reservoir-like recession dynamics are already compatible with the LSTM architecture.

However, this correspondence does not make the storage-discharge relationship explicit. The learned cell state is not required to represent catchment storage, and predicted discharge is not required to scale with that state. A linear reservoir constraint, $Q = KS$, therefore could provide a lightweight way to formalise a physically meaningful relationship that the LSTM can already approximate, while still allowing flexibility to fit the observed hydrograph. Although real catchments often exhibit multiple storage pathways and nonlinear recession behaviour (Clark et al., 2009; Harman et al., 2009), a single exponential store provides a useful first-order description of rapid drainage at sub-daily scales (Harman et al., 2009; Kirchner, 2009).

Existing physics-informed hydrological LSTMs have mainly imposed mass conservation architecturally (Hoedt et al., 2021), embedded conceptual model structures (Acuña Espinoza et al., 2024; Feng et al., 2022), or applied soft storage-discharge penalties at daily resolution (Pokharel et al., 2023). To our knowledge, no large-sample study has tested a learnable storage-discharge constraint within an LSTM at sub-daily resolution, where recession dynamics are explicitly resolved. This gap is important because multi-timescale LSTMs have only recently been demonstrated for rainfall-runoff prediction (Gauch et al., 2021), and the value of a recession-based physical constraint should depend on whether recession dynamics are visible at the modelling timestep.

We address this gap using two large-sample datasets at sub-daily resolution: CAMELS-NZ (Bushra et al., 2025) which provides hourly streamflow and disaggregated hourly precipitation for 369 catchments across New Zealand, and CAMELS-GB (Coxon et al., 2020; Coxon et al., 2025) which also provides hourly streamflow and gauge-based hourly precipitation for Great Britain. After quality-control screening, 174 New Zealand and 519 Great Britain catchments were retained for analysis. Building on the NeuralHydrology framework (Kratzert et al., 2022) developed by Kratzert, Klotz, Nearing and colleagues (which established LSTMs as the state of the art for rainfall-runoff modelling (Kratzert et al., 2018; Kratzert et al., 2019a; Kratzert et al., 2019b)), we augment the CudaLSTM architecture (Kratzert et al., 2022) with a learned linear reservoir constraint (Q = KS) and its nonlinear extension ($Q = KS^n$), where K and n are learnable parameters that emerge during training (Fig. 1b). Unlike approaches that enforce physical structure through architectural redesign (Acuña Espinoza et al., 2024; Frame et al., 2023; Hoedt et al., 2021; Höge et al., 2022), we retain the standard LSTM architecture and introduce physics through a lightweight storage-discharge regularisation term. The strength of this regularisation is controlled by λ, which weights the physics loss relative to the streamflow prediction loss. Both models are trained on identical forcing, so any difference in skill is attributable to the storage-discharge constraint rather than to input information. We deliberately use precipitation as the sole dynamic forcing as runoff in steep, wet catchments is precipitation-dominated, and the recession dynamics the constraint targets are well resolved by precipitation and discharge alone, so a minimalist forcing yields the cleanest test of the constraint.

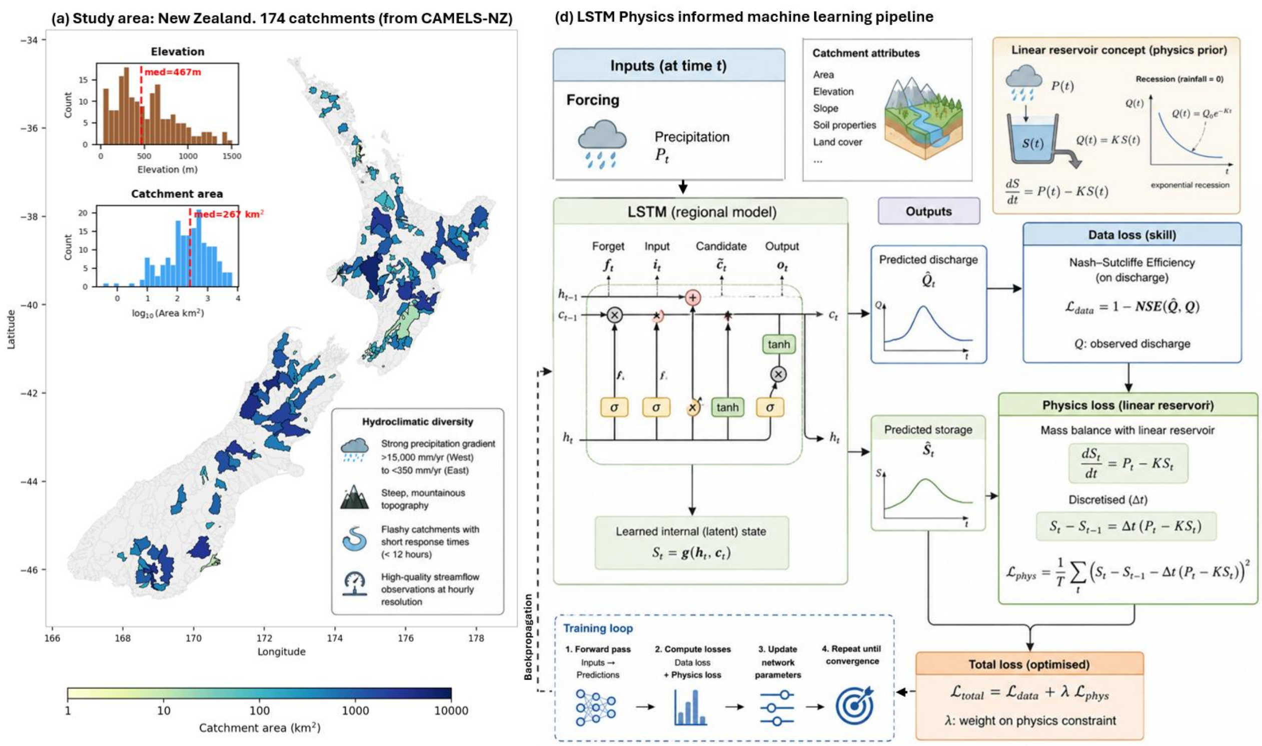

Figure 1. Study catchments and physics-informed LSTM modelling framework. (a) The 174 CAMELS-NZ catchments used in this study, coloured by drainage area, spanning New Zealand's hydroclimatic gradient. Histograms show the distributions of catchment elevation and drainage area; dashed red lines indicate the median values. (b) Physics-informed LSTM workflow. Hourly precipitation and static catchment attributes are passed to a CudaLSTM, which predicts discharge and a latent storage state. Model training combines a data loss based on Nash–Sutcliffe Efficiency with a soft physics loss that penalises deviations from a storage–discharge reservoir relationship. The linear reservoir form is Q = KS; the nonlinear extension $Q = KS^n$ is evaluated separately but is not shown in the schematic.

New Zealand presents a distinctive testbed. Its steep, flashy catchments often exhibit concentration times of less than 12 h (Bushra et al., 2025), its hydroclimate exhibits a strong west-east precipitation gradient (>15,000 mm yr^{-1} on the west coast versus <350 mm yr^{-1} in eastern rain shadows), and national-scale physics-based hydrological models exhibit substantial variation in performance across catchments (Cattoën et al., 2025; McMillan et al., 2016). Recent work has introduced machine-learning methods for New Zealand river-flow prediction at a single catchment (Ardid et al., 2024). We therefore use New Zealand to investigate the physical plausibility and extrapolation behaviour of the learned constraint, and Great Britain as an external replication using gauge-based hourly precipitation. Specifically, we examine the learned physics parameters, analyse where the constraint provides the greatest benefit relative to event novelty, evaluate robustness under out-of-sample forcing (outside the observed training range), and compare performance at hourly and daily resolution to isolate the role of temporal resolution.

Methods

Study area and datasets

The primary dataset is CAMELS-NZ (Bushra et al., 2025), which provides hourly streamflow and precipitation (used here), among other variables, for 369 catchments across New Zealand, spanning 1972-2024. Catchments cover New Zealand's full hydroclimatic gradient, from extremely wet west-coast Alpine catchments receiving >10,000 mm/yr precipitation to semi-arid eastern plains with <500 mm/yr, with drainage areas ranging from a few km² to approximately 6,000 km². Geological substrates include greywacke, schist, volcanic, plutonic, hard and soft sedimentary formations, and alluvium. We applied quality control screening requiring no more than 20% missing data fraction across the full record period, yielding 174 accepted catchments with good spatial coverage across both North and South Islands.

Forcing data consist of hourly precipitation derived from the Virtual Climate Station Network (VCSN) (Tait et al., 2006), a 5-km thin-plate-spline interpolation of approximately 400-1,400 rain gauges, disaggregated to hourly resolution using multiplicative random cascades (Rupp et al., 2009). We note that this disaggregation means the sub-daily timing of precipitation may not be fully accurate. Static catchment attributes include drainage area (km²), mean elevation (m), mean slope (m/m), mean annual precipitation (mm/yr), aridity index, and forest fraction, sourced from the CAMELS-NZ attribute tables.

For the daily-resolution experiment, hourly data are aggregated to daily totals (precipitation, with a minimum of 18 valid hours required per day) and daily means (discharge). This ensures that the same physical catchments and observation periods are compared across resolutions, isolating the effect of temporal aggregation.

Great Britain. We use CAMELS-GB (Coxon et al., 2020), which provides gauge-based hourly precipitation (CAMELS-GB v2r) (Coxon et al., 2025) and hourly streamflow. CAMELS-GB v2r is a 1 km gridded product in which the daily CEH-GEAR rainfall total is temporally disaggregated using interpolated hourly rain-gauge observations (with a design-storm fallback in gauge-sparse cells), so its sub-daily timing is grounded in real hourly measurements rather than a stochastic cascade. Catchments were screened with the same criteria applied to New Zealand (≤20% missing data in the hourly streamflow record and ≥10 valid years) yielding 519 catchments. Daily-resolution experiments aggregate the identical hourly streamflow to daily means and use daily precipitation totals, so that hourly and daily results are compared on the same catchments.

LSTM architecture

We employ the CudaLSTM architecture implemented in the NeuralHydrology framework (Kratzert et al., 2022), a widely used open-source library for deep learning in hydrology. The model receives hourly (or daily) precipitation as dynamic input, producing streamflow predictions at the corresponding resolution. The architecture consists of a single LSTM layer with 128 hidden units, a linear regression head, and linear output activation.

Training hyperparameters are held constant across all experiments: 30 epochs, Adam optimiser with initial learning rate 0.001 (halved at epoch 15), batch size 256, and gradient clipping at norm 1.0. The sequence length is 336 hours (14 days) for hourly models and 365 days for daily models, with prediction at the final timestep only (predict_last_n = 1). The loss function is the negative Nash-Sutcliffe Efficiency (NSE), computed with per-basin target standard deviation normalisation using an epsilon of 0.1 to prevent numerical instability for low-variance basins.

Per-basin models were trained for all experiments. For each catchment in the primary New Zealand hourly experiment, we trained one baseline LSTM and twelve physics-informed variants, comprising six λ values for each of two reservoir formulations (linear and nonlinear). This produced $13 \times 174 = 2{,}262$ trained models. Equivalent ensembles were trained for the remaining experiments: 1,044 New Zealand daily linear-physics models plus one regional baseline model, 3,794 Great Britain hourly models, and 7,046 Great Britain daily models. In total, approximately 14,000 models were trained. This design enables per-basin optimisation of the regularisation strength and reservoir formulation while isolating the effect of the physics constraint from cross-catchment transfer learning.

Physics-informed loss function

The linear reservoir model describes the storage-discharge relationship as $Q = KS$, where Q is discharge, S is catchment storage, and K is the recession coefficient (time^{-1}). Combined with the water balance equation $dS/dt = P - Q$ (neglecting evapotranspiration, which varies slowly relative to storm dynamics), this yields first-order exponential recession dynamics with e-folding time $\tau = 1/K$.

We implement this as a soft constraint by augmenting the standard NSE loss:

$$L\_total = L\_NSE + \lambda \cdot L\_physics$$

where L_physics quantifies departures from linear reservoir behaviour and λ controls the regularisation strength. The physics loss is computed as follows: the LSTM produces a storage head output S(t) alongside the discharge prediction Q(t). The time derivative dS/dt is estimated via ordinary least squares over 10-timestep sliding windows. Precipitation P is un-normalised using per-basin statistics (mean and standard deviation computed from the training data) so that the water balance $dS/dt = P - KS$ is evaluated in physical units. The physics loss penalises the residual $||dS/dt - (P - KS)||^2$ averaged over the prediction window.

The recession coefficient K is parameterised as K = exp(log_K), ensuring positivity, with log_K as a learnable parameter initialised at $K\_0 = 0.018$ h^{-1} (hourly, corresponding to $\tau \approx 56$ hours) or $K\_0 = 0.05$ day^{-1} (daily, corresponding to $\tau = 20$ days). This log-parameterisation stabilises training by preventing K from becoming negative or excessively large.

We additionally evaluate a nonlinear reservoir extension $Q = KS^n$ where the exponent n is a learnable parameter initialised at 1.0. When $n = 1$, this reduces to the linear case. This formulation follows previous ones that showed that storage-discharge relationships in real catchments generally follow power-law behaviour (Harman et al., 2009).

Experimental design

Lambda sweep. For each catchment, we train seven models: one baseline LSTM ($\lambda = 0$) and six physics-informed variants with $\lambda \in [0.01, 0.1, 1.0, 10.0, 100.0, 1000.0]$. This per-basin sweep design allows identification of the optimal regularisation strength for each catchment individually and subsequent investigation of what catchment properties predict the optimal λ. The best λ per basin is selected by test-period NSE.

Resolution comparison. The same New Zealand catchments are evaluated at both hourly and daily resolution using identical architecture, physics constraint, and lambda sweep. The only difference is the temporal aggregation of forcing and target data, ensuring that any performance differences are attributable to resolution rather than experimental design choices.

Evaluation of metrics. Performance is evaluated using the Nash-Sutcliffe Efficiency (NSE) computed over the test period at the native temporal resolution. NSE is chosen as the primary metric for consistency with the broader CAMELS literature. The primary comparison metric is $\Delta NSE = NSE\_physics(best\ \lambda) - NSE\_baseline$, representing the per-basin skill change from adding the physics constraint. We additionally decompose performance by flow regime, defining three regimes based on the observed flow distribution: low flow ($Q < Q25$), normal flow ($Q25 \leq Q \leq Q95$), and high flow ($Q > Q95$). Regime-specific NSE is computed independently for each flow class.

Lambda prediction from catchment properties. To investigate whether optimal regularisation strength can be predicted a priori - a prerequisite for applying the framework at ungauged sites - we fit a log-linear regression: $\log10(\lambda) = a \cdot \log10(A) + b$, where A is catchment area (km^2). Predictability is evaluated using Spearman rank correlation, ordinary least squares R^2, and leave-one-out cross-validation (LOO-CV). In LOO-CV, each catchment is held out in turn, the regression is re-fitted on the remaining catchments, λ is predicted for the held-out catchment, and performance is evaluated using the sweep run closest to the predicted λ. The resulting λ-area relationship and its cross-validated skill are shown in Supplementary Fig. S4.

Results

Our physics-informed LSTM substantially improves hourly streamflow prediction across New Zealand. The baseline model, trained using precipitation as the sole dynamic forcing, achieves a median test-period NSE of 0.30 across 174 catchments (exceeding the average uncalibrated daily NSE of 0.16 reported for New Zealand's national TopNet model (McMillan et al., 2016)). Adding the linear reservoir constraint ($Q = KS$) as a soft regularisation term raises the median NSE to 0.44 and improves performance in 172 of 174 catchments (Fig. 2). The two catchments that do not improve are high-elevation, snowmelt-influenced South Island headwaters where the unconstrained baseline already performs poorly (e.g., Mary Burn at Mt MacDonald in the Mackenzie Basin).

The improvement is spatially widespread across New Zealand's hydroclimatic and geological gradients (Fig. 2a-d). The median change in NSE is +0.15. The largest gains occur where the baseline model is weakest (Supplementary Fig. S1; see also the comprehensive parameter summary in Supplementary Fig. S9), suggesting that the storage-discharge constraint is most useful where the unconstrained LSTM has difficulty learning recession behaviour from the available data. Catchment area is related to baseline skill but only weakly related to the physics benefit itself (Supplementary Fig. S6; Supplementary Table 2), indicating that the constraint does not simply favour small or large basins. The distribution of the regularisation weight (that controls the strength of the physics loss relative to the streamflow prediction loss) is shown in Fig. 2d.

Performance gains are concentrated in the flow regimes most relevant to hydrograph volume and flood prediction (Supplementary Fig. S2 and Supplementary Table 1). In the normal-flow regime 92% of catchments improve, with a median NSE of +0.50. In the high-flow regime, 87% improve, with a median NSE of +0.17. Low-flow skill is largely unchanged.

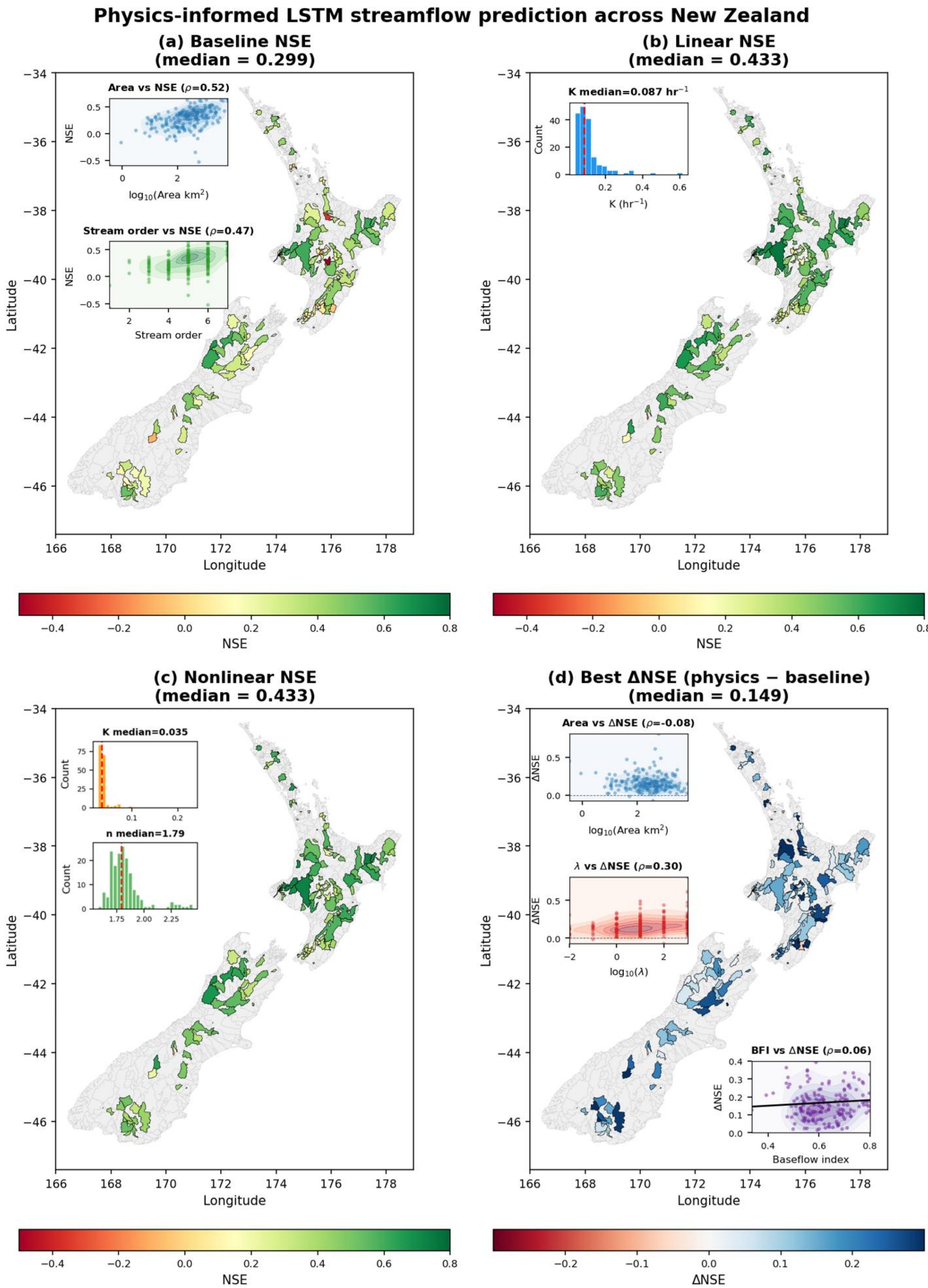

Figure 2. Hourly-resolution performance and learned parameters across New Zealand. (a) Baseline LSTM NSE (median = 0.3) with area-vs-NSE and stream-order scatter insets. (b) Linear physics-informed NSE (median = 0.433) with learned K distribution inset (K median = 0.087 h⁻¹). (c) Nonlinear physics-informed NSE (median = 0.435) with K and n distribution insets (n median = 1.79). (d) Best ΔNSE (physics minus baseline; median = +0.150) with area-vs-ΔNSE, λ-vs-ΔNSE and BFI-vs-ΔNSE scatter insets. λ denotes the weighting applied to the physics-constraint term in the loss function.

Learned physics parameters

The physics-informed model learns physically plausible recession dynamics without direct supervision on storage or recession parameters (Fig. 3). The learned recession coefficient (K) has a median of 0.087 h^{-1} across New Zealand catchments, corresponding to an e-folding recession timescale (tau = 1/K) ~ 11.5 h (e-folding is the time required for storage to fall to about 37% of its initial value under rainless conditions). This timescale is of the same order as the rapid sub-daily response expected in steep New Zealand catchments, where flood concentration times are often shorter than 12 h (Bushra et al., 2025). Because (K) is learned inside the model rather than fitted independently from observed recession curves, we interpret it as an effective model timescale rather than a direct estimate of the catchment recession constant. The distribution and spatial pattern of the learned K values are shown in Supplementary Fig. S5.

Individual learned (K) values range from 0.035 to 0.61 h^{-1}, indicating that the constraint allows substantial variation in effective recession timescale across catchments. The learned storage dynamics (S(t)) track an independent water-balance proxy based on 90-day rolling cumulative (Q-P) (Fig. 3d–f), suggesting that the constrained LSTM encodes a storage-like latent state rather than an arbitrary internal variable. The nonlinear reservoir extension ($Q = KS^n$) yields a learned exponent clustering near n = 1.79, but provides only marginal additional predictive benefit over the linear reservoir (median NSE 0.435 versus 0.433; Fig. 2c; Supplementary Fig. S7) reduce physically implausible saturation in the model response to extreme precipitation forcing.

Behaviour under novel recession and forcing conditions

We tested whether the physics constraint improves model behaviour when the test period contains hydrological conditions that are weakly represented during training. First, we quantified recession novelty as the difference between test-period flood recession timescales and the closest recession timescales observed during training. Catchments with more novel test-period recessions tend to show larger physics-informed improvements (Supplementary Fig. S3; Spearman $\rho = 0.251$, $p = 0.0009$; this remains after controlling for baseline model skill, partial $\rho = 0.38$).

In addition, we used a synthetic storm-scaling experiment to examine how the models respond to precipitation forcing outside the observed range. For an example catchment, precipitation was multiplied by factors of 1.0, 1.5, and 2.0 while the trained models were held fixed. The physics-informed models produced a stronger and more nearly proportional increase in peak discharge than the unconstrained LSTM, whereas the baseline response tended to saturate at high forcing (Supplementary Fig. S3). This shows that the storage-discharge constraint can improve behaviour under out-of-sample forcing conditions.

A second large-sample test in Great Britain at hourly resolution

To test whether the hourly physics benefit extends beyond New Zealand, and whether it depends on the CAMELS-NZ precipitation disaggregation, we repeated the experiment using CAMELS-GB (Coxon et al., 2020; Coxon et al., 2025). Great Britain provides a useful comparison because its hourly precipitation product is informed by hourly rain-gauge observations (Coxon et al., 2025), whereas CAMELS-NZ hourly precipitation is derived from daily rainfall using multiplicative random cascades (Bushra et al., 2025; Rupp et al., 2009). Applying the same quality-control criteria used for New Zealand, no more than 20% missing data in the hourly record and at least 10 valid years, retained 519 catchments.

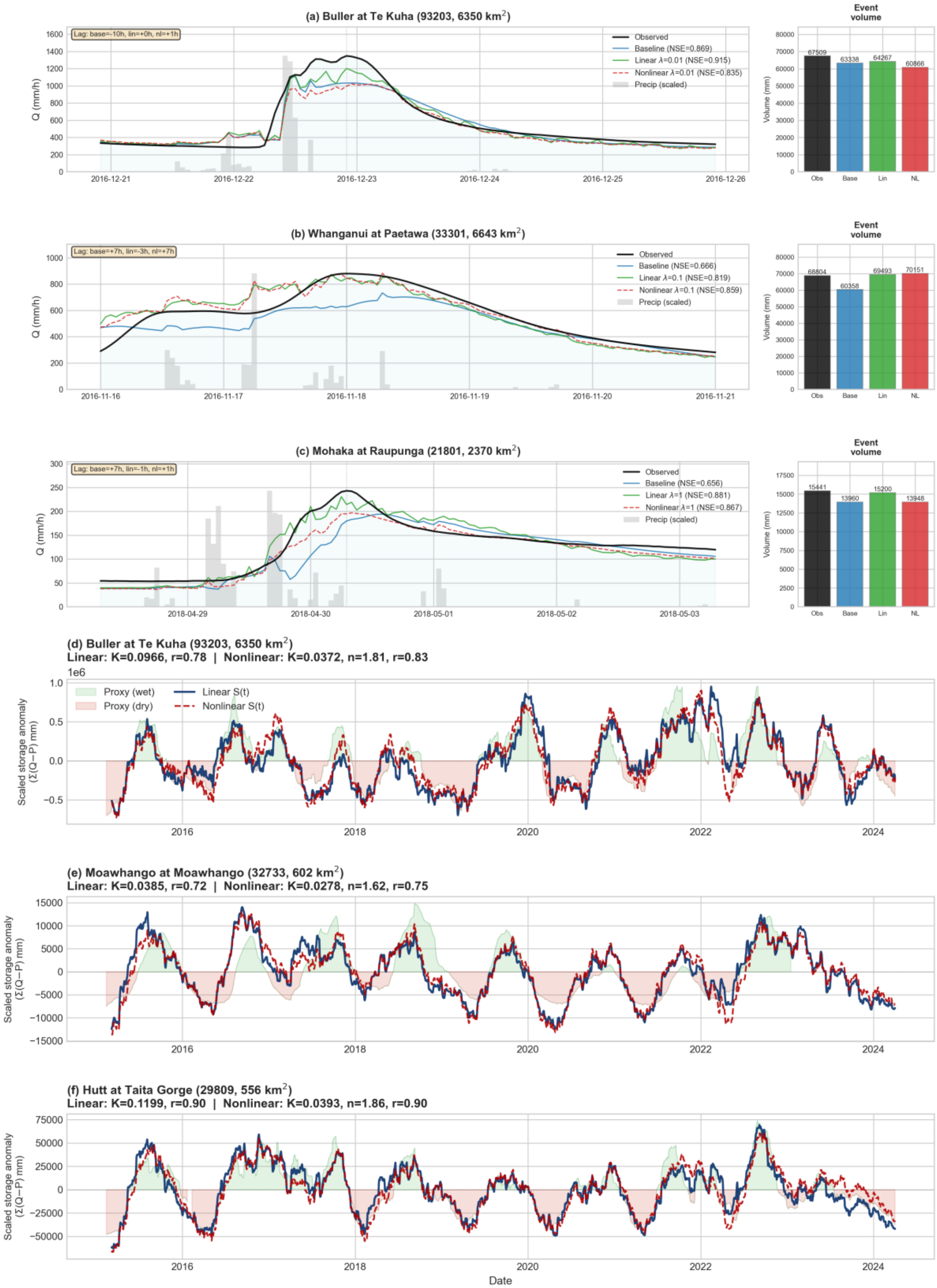

Figure 3. Representative hourly hydrographs and learned storage dynamics. Top panels show observed (black), baseline (blue), and physics-informed (red) discharge for selected catchments spanning the performance spectrum. Bottom panels show learned storage S(t) compared with the water-balance proxy (90-day rolling cumulative Q-P), demonstrating that the LSTM encodes physically meaningful catchment storage without explicit supervision.

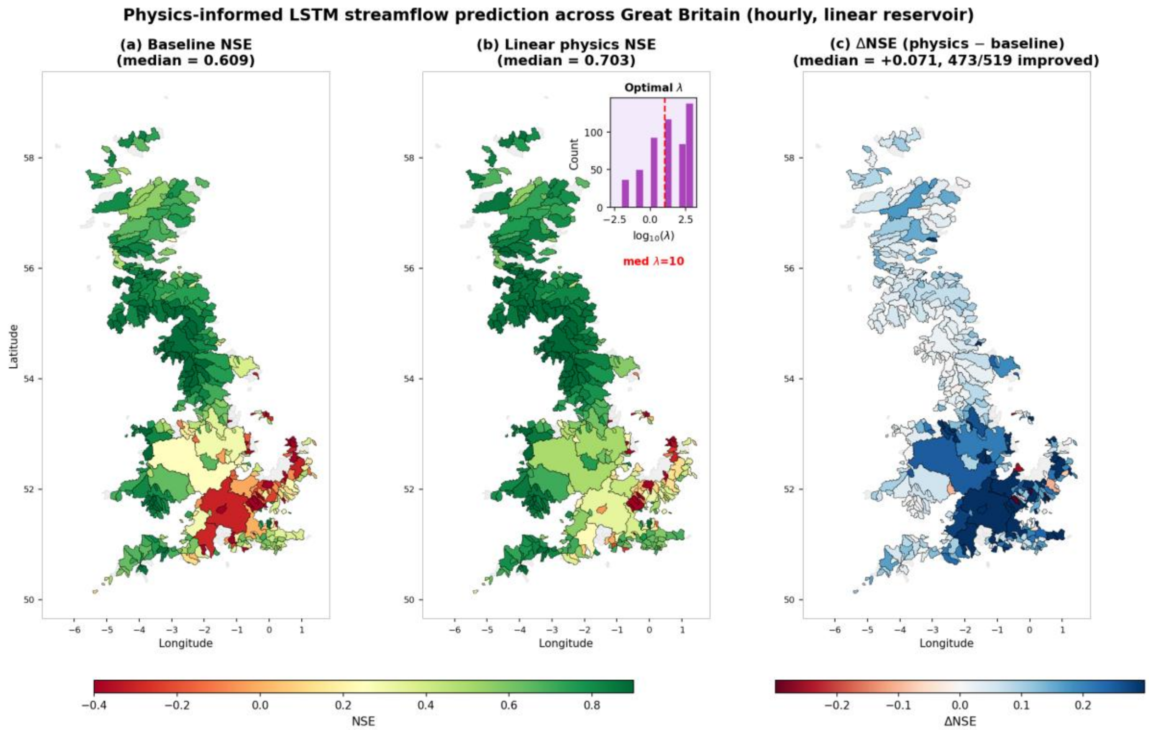

Figure 4. Physics-informed LSTM streamflow prediction across Great Britain (hourly, linear reservoir). (a) Baseline LSTM NSE (median 0.61). (b) Linear physics-informed NSE (median 0.70) with the distribution of optimal regularisation weight λ inset (median λ = 10). (c) Best physics improvement ΔNSE = physics − baseline (median +0.07; 473 of 519 catchments improved). Catchments are screened to the same ≤20% hourly-missing, ≥10-year criteria as New Zealand; GB uses gauge-based (CAMELS-GB v2r) hourly precipitation, whose sub-daily timing reflects interpolated hourly rain-gauge observations, so the result is not an artefact of stochastic disaggregation.

At hourly resolution, the linear reservoir constraint improves 91% of Great Britain catchments (Fig. 4), increasing the median NSE from 0.61 to 0.70. When the same Great Britain catchments, model architecture, and physics constraint are evaluated at daily resolution, the benefit largely disappears, with only 21% of catchments improving (Supplementary Fig. S8). This suggests that the hourly improvement is not simply an artefact of the New Zealand precipitation data. The same pattern occurs in both countries: the storage-discharge constraint helps at hourly resolution but provides little benefit at daily resolution.

As in New Zealand, in Great Britain the gain is largest where the baseline model is weakest (Spearman ρ between baseline NSE and ΔNSE = -0.68). By flow regime, the benefit is strongest in the parts of the hydrograph most relevant to flood prediction. In Great Britain, median ΔNSE is +0.19 in the normal-flow regime, with 85% of catchments improved, and +0.16 in the high-flow regime, with 81% of catchments improved (Supplementary Table 1).

Across both countries, the strongest predictor of improvement is baseline model skill. NSE correlates negatively with baseline NSE in both New Zealand (ρ = -0.58) and Great Britain (ρ = -0.68). Hydrological signatures add little explanatory power in New Zealand, where nearly all catchments improve, but show a clearer secondary signal in Great Britain, where improvements are more selective. In Great Britain, gains are larger in baseflow-dominated catchments and smaller in flashy, surface-runoff catchments (Supplementary Fig. S1).

Discussion and Conclusions

The physics loss does more than improve NSE. It encourages one learned LSTM state to behave like catchment storage and links that state to discharge through an effective recession timescale. This matters because the constraint targets recession behaviour, which is central to flood prediction, while leaving the rest of the LSTM flexible enough to fit the observed hydrograph. The learned (K) should therefore be viewed as a model-scale memory parameter, not as a direct recession constant fitted from observed hydrographs.

The nonlinear reservoir experiment clarifies what information the physics loss contributes. Although the learned exponents are consistent with evidence that catchment-scale recession behaviour can emerge from heterogeneous storage domains and multiple drainage timescales (Clark et al., 2009; Gnann et al., 2021; Harman et al., 2009), the nonlinear model adds little predictive skill relative to the linear reservoir (Supplementary Fig. S7). This suggests that the first-order control on hourly flood prediction is catchment memory, rather than the detailed shape of the storage-discharge relationship. Once this memory timescale is represented, additional storage–discharge complexity contributes comparatively little to NSE in these experiments.

The usefulness of a physics constraint depends on whether the constrained process is resolved by the observational timestep. At hourly resolution, recession events span many timesteps, so the storage-discharge loss receives information about the shape and duration of recession limbs. At daily resolution, the same recession dynamics are compressed into only a few values (Supplementary Fig. S8). The constraint then has much less information with which to regularise the model, and the imposed storage-discharge relationship can become a poorer match to the effective daily-scale dynamics. This explains why the physics constraint helps at hourly resolution but provides little benefit at daily resolution in both countries. It also places the daily-resolution literature in context. Mass-conserving LSTMs, differentiable HBV models, and hybrid HBV-LSTM approaches have generally performed similarly to, or slightly worse than, unconstrained LSTMs on daily CAMELS-style benchmarks (Acuña Espinoza et al., 2024; Acuña Espinoza et al., 2025; Feng et al., 2022; Hoedt et al., 2021). Our results suggest that this limited improvement may partly reflect the timestep of the benchmark datasets, rather than a general failure of physics-informed learning. A constraint can only help if the process it represents is visible at the resolution used for training and evaluation.

The Great Britain experiment shows that the hourly benefit is not specific to New Zealand or to the CAMELS-NZ precipitation disaggregation. Despite differences in hydroclimate, topography, baseline skill, and precipitation data, both countries show the pattern that storage-discharge constraint improves most catchments at hourly resolution, but provides little benefit at daily resolution. Because both models use the same forcing within each experiment, the relative improvement isolates the effect of the storage-discharge constraint more directly than the absolute NSE. The supporting extrapolation analyses are consistent with this interpretation. Catchments whose test-period recessions differ most from training-period recessions tend to show larger physics-informed improvements, and synthetic storm scaling shows that the constrained model avoids some of the peak-flow saturation seen in the unconstrained LSTM. These results should be viewed as secondary evidence, because the recession-novelty relationship is modest and the storm-scaling experiment is a controlled stress test rather than a full forecast experiment. They nevertheless support the idea that the constraint is most useful when the model encounters recession behaviour that is weakly represented in the training data.

For operational flood forecasting, the main implication is that physics-informed deep learning is most likely to add value in sub-daily systems where recession dynamics and flood timing are explicitly resolved. This is relevant for systems such as the Aotearoa Flood Awareness System, which operates at hourly resolution using TopNet (Cattoën et al., 2025). A physics-informed LSTM would not replace process-based modelling, but it could provide a complementary data-driven model with interpretable recession parameters and improved robustness in catchments where the unconstrained LSTM struggles.

Several extensions follow directly from the limitations of the present formulation. First, the model currently learns a stationary (K), although recession behaviour can vary with catchment wetness, season, vegetation state, and snow processes (Kirchner, 2009). A natural next step is to learn a dynamic K(S) or K(t), that changes with catchment state while retaining physical interpretability. Second, the single-reservoir structure could be extended to multiple coupled reservoirs representing fast and slow drainage pathways (Acuña Espinoza et al., 2024; Clark et al., 2009; Feng et al., 2022; Harman et al., 2009). Third, the method could be evaluated in operational forecast mode with numerical weather prediction ensembles, and under non-stationary conditions such as land-use or climate change impacts (Cattoën et al., 2025; Feng et al., 2023).

Broader large-sample evaluation will require suitable sub-daily datasets. Many CAMELS datasets, including Australia, Brazil, Chile, and Germany, currently provide daily forcing and streamflow for large-sample benchmarking (Alvarez-Garreton et al., 2018; Chagas et al., 2020; Fowler et al., 2021; Loritz et al., 2024). The results here suggest that repeating the same storage-discharge constraint at daily resolution is unlikely to produce large gains. The more informative next test should be a complete sub-daily evaluation in additional hydroclimatic regions.

Acknowledgments

Author Contributions: A.A. and D.D. conceived the study and developed the modelling pipeline, including designing the physics-informed LSTM. A.A. performed the analyses, and led the writing of the manuscript. C.C. provided the New Zealand hydrometeorological data and hydrological expertise. M.P. contributed to the methodology and interpretation. All authors discussed the results and contributed to the manuscript.

Conflict of Interest Statement: The authors declare no conflicts of interest relevant to this study.

Open Research Section

Data Availability Statement: The hydrometeorological time series and catchment attributes analysed in this study are openly available from their original sources. CAMELS-NZ, providing hourly streamflow and precipitation for New Zealand, is described by Bushra et al. (2025). CAMELS-GB, providing streamflow and catchment attributes for Great Britain, is available from the NERC Environmental Information Data Centre (Coxon et al., 2020), and the gauge-based hourly precipitation product (CAMELS-GB v2r) (Coxon et al., 2025). The per-basin results generated in this study - baseline and physics-informed NSE, learned recession parameters (K and n), and the optimal regularisation strength for each catchment - are provided as supplementary data.

Code Availability: The physics-informed LSTM is implemented as an extension of the open-source NeuralHydrology framework (Kratzert et al., 2022) (https://github.com/neuralhydrology/neuralhydrology). The code implementing the linear and nonlinear reservoir physics loss, the per-basin training and λ-sweep pipeline, and the scripts used to compute the hydrological signatures and generate the figures will be deposited in a public repository (Zenodo) on publication. To make the method easy to inspect and reuse, the paper also includes a lightweight, self-contained demonstration that depends only on standard scientific-Python packages (NumPy, pandas, PyTorch, Matplotlib) and does not require installation of the full framework. The demonstration trains a baseline LSTM and a physics-informed LSTM with the linear storage-discharge constraint ($Q = KS$) on a single example catchment (Awanui at School Cut, CAMELS-NZ), and produces the observed-versus-baseline-versus-physics streamflow comparison, including a hydrograph for a representative flood event and the learned storage state. Bundled hourly input data for the example catchment are included so the demonstration runs end-to-end.

References

Acuña Espinoza, E., Loritz, R., Álvarez Chaves, M., Bäuerle, N., & Ehret, U. (2024). To bucket or not to bucket? Analyzing the performance and interpretability of hybrid hydrological models with dynamic parameterization. *Hydrol. Earth Syst. Sci.*, **28**, 2705-2719.

Acuña Espinoza, E., Loritz, R., Kratzert, F., Klotz, D., Gauch, M., Álvarez Chaves, M., & Ehret, U. (2025). Analyzing the generalization capabilities of a hybrid hydrological model for extrapolation to extreme events. *Hydrol. Earth Syst. Sci.*, **29**, 1277-1294.

Alvarez-Garreton, C. et al. (2018). The CAMELS-CL dataset: catchment attributes and meteorology for large sample studies - Chile dataset. *Hydrol. Earth Syst. Sci.*, **22**, 5817-5846.

Ardid, A., Pahlow, M. & Dempsey, D. (2024). Integrating machine learning into hydrology education with a focus on river flow modelling. *J. Hydrol. N. Z.*, **63**, 69-85.

Bushra, S., Shakya, J., Cattoën, C., Fischer, S. & Pahlow, M. (2025). CAMELS-NZ: hydrometeorological time series and landscape attributes for New Zealand. *Earth Syst. Sci. Data*, **17**, 5745-5760.

Cattoën, C., Conway, J., Fedaeff, N., Lagrava, D., Blackett, P. et al. (2025). A national flood awareness system for ungauged catchments in complex topography: The case of development, communication and evaluation in New Zealand. *J. Flood Risk Manag.*, **18**, e12864.

Chagas, V. B. P. et al. (2020). CAMELS-BR: Hydrometeorological time series and landscape attributes for 897 catchments in Brazil. *Earth Syst. Sci. Data*, **12**, 2075-2096.

Clark, M. P., Rupp, D. E., Woods, R. A., Tromp-van Meerveld, H. J., Peters, N. E. & Freer, J. E. (2009). Consistency between hydrological models and field observations: linking processes at the hillslope scale to hydrological responses at the watershed scale. *Hydrological Processes*, **23**, 311-319.

Coxon, G., Addor, N., Bloomfield, J. P., Freer, J., Fry, M. et al. (2020). CAMELS-GB: hydrometeorological time series and landscape attributes for 671 catchments in Great Britain. *Earth Syst. Sci. Data*, **12**, 2459-2483.

Coxon, G., Zheng, Y., Barbedo, R., Cooper, H., Fileni, F., Fowler, H. J., ... & Wendt, D. E. (2025). CAMELS-GB v2: hydrometeorological time series and landscape attributes for 671 catchments in Great Britain. *Earth System Science Data Discussions*, **2025**, 1-44.

De la Fuente, L. A., Ehsani, M. R., Gupta, H. V. & Condon, L. E. (2024). Toward interpretable LSTM-based modeling of hydrological systems. *Hydrol. Earth Syst. Sci.*, **28**, 945-971.

Feng, D., Liu, J., Lawson, K. & Shen, C. (2022). Differentiable, learnable, regionalized process-based models with multiphysical outputs can approach state-of-the-art hydrologic prediction accuracy. *Water Resour. Res.*, **58**, e2022WR032404.

Feng, D., Beck, H., Lawson, K. & Shen, C. (2023). The suitability of differentiable, physics-informed machine learning hydrologic models for ungauged regions and climate change impact assessment. *Hydrol. Earth Syst. Sci.*, **27**, 2357-2373.

Fowler, K. J. A., Acharya, S. C., Addor, N., Chou, C. & Peel, M. C. (2021). CAMELS-AUS: hydrometeorological time series and landscape attributes for 222 catchments in Australia. *Earth Syst. Sci. Data*, **13**, 3847-3867.

Frame, J. M. et al. (2022). Deep learning rainfall-runoff predictions of extreme events. *Hydrol. Earth Syst. Sci.*, **26**, 3377-3392.

Frame, J. M., Kratzert, F., Gupta, H. V., Ullrich, P. & Nearing, G. S. (2023). On strictly enforced mass conservation constraints for modelling the rainfall-runoff process. *Hydrol. Process.*, **37**, e14847.

Gauch, M., Kratzert, F., Klotz, D., Nearing, G., Lin, J. et al. (2021). Rainfall-runoff prediction at multiple timescales with a single Long Short-Term Memory network. *Hydrol. Earth Syst. Sci.*, **25**, 2045-2062.

Gnann, S. J., Coxon, G., Woods, R. A., Howden, N. J. K. & McMillan, H. K. (2021). TOSSH: A Toolbox for Streamflow Signatures in Hydrology. *Environ. Model. Softw.*, **138**, 104983.

Harman, C. J., Sivapalan, M. & Kumar, P. (2009). Power law catchment-scale recessions arising from heterogeneous linear small-scale dynamics. *Water Resour. Res.*, **45**, W09404.

Hoedt, P.-J. et al. (2021). MC-LSTM: Mass-Conserving LSTM. *Proc. Mach. Learn. Res.*, **139**, 4275-4286.

Höge, M., Scheidegger, A., Baity-Jesi, M., Albert, C. & Fenicia, F. (2022). Improving hydrologic models for predictions and process understanding using neural ODEs. *Hydrol. Earth Syst. Sci.*, **26**, 5085-5102.

Karniadakis, G. E. et al. (2021). Physics-informed machine learning. *Nat. Rev. Phys.*, **3**, 422-440.

Kirchner, J. W. (2009). Catchments as simple dynamical systems: Catchment characterization, rainfall-runoff modeling, and doing hydrology backward. *Water Resour. Res.*, **45**, W02429.

Kratzert, F., Klotz, D., Brenner, C., Schulz, K. & Herrnegger, M. (2018). Rainfall-runoff modelling using Long Short-Term Memory (LSTM) networks. *Hydrol. Earth Syst. Sci.*, **22**, 6005-6022.

Kratzert, F. et al. (2019a). Toward improved predictions in ungauged basins: Exploiting the power of machine learning. *Water Resour. Res.*, **55**, 11344-11354.

Kratzert, F., Klotz, D., Shalev, G., Klambauer, G., Hochreiter, S. & Nearing, G. (2019b). Towards learning universal, regional, and local hydrological behaviors via machine learning applied to large-sample datasets. *Hydrol. Earth Syst. Sci.*, **23**, 5089-5110.

Kratzert, F., Gauch, M., Nearing, G. & Klotz, D. (2022). NeuralHydrology - A Python library for Deep Learning research in hydrology. *J. Open Source Softw.*, **7**, 4050.

Lees, T., Buechel, M., Anderson, B., Slater, L., Reece, S. et al. (2021). Benchmarking data-driven rainfall-runoff models in Great Britain: a comparison of long short-term memory (LSTM)-based models with four lumped conceptual models. *Hydrol. Earth Syst. Sci.*, **25**, 5517-5534.

Lees, T. et al. (2022). Hydrological concept formation inside long short-term memory (LSTM) networks. *Hydrol. Earth Syst. Sci.*, **26**, 3079-3101.

Loritz, R. et al. (2024). CAMELS-DE: hydro-meteorological time series and attributes for 1582 catchments in Germany. *Earth Syst. Sci. Data*, **16**, 5625-5642.

Mai, J. et al. (2022). The Great Lakes Runoff Intercomparison Project Phase 4: The Great Lakes (GRIP-GL). *Hydrol. Earth Syst. Sci.*, **26**, 3537-3572.

McMillan, H. K., Booker, D. J. & Cattoën, C. (2016). Validation of a national hydrological model. *J. Hydrol.*, **541**, 800-815.

Nearing, G. S. et al. (2021). What role does hydrological science play in the age of machine learning? *Water Resour. Res.*, **57**, e2020WR028091.

Nearing, G. S. et al. (2024). Global prediction of extreme floods in ungauged watersheds. *Nature*, **627**, 559-563.

Pokharel, S., Roy, T. & Admiraal, D. (2023). Effects of mass balance, energy balance, and storage-discharge constraints on LSTM for streamflow prediction. *Environ. Model. Softw.*, **166**, 105730.

Rupp, D. E., Keim, R. F., Ossiander, M., Brugnach, M. & Selker, J. S. (2009). Time scale and intensity dependency in multiplicative cascades for temporal rainfall disaggregation. *Water Resour. Res.*, **45**, W07409.

Shen, C. et al. (2023). Differentiable modelling to unify machine learning and physical models for geosciences. *Nat. Rev. Earth Environ.*, **4**, 552-567.

Tait, A., Henderson, R., Turner, R. & Zheng, X. (2006). Thin plate smoothing spline interpolation of daily rainfall for New Zealand using a climatological rainfall surface. *Int. J. Climatol.*, **26**, 2097-2115.

Willard, J., Jia, X., Xu, S., Steinbach, M. & Kumar, V. (2022). Integrating scientific knowledge with machine learning for engineering and environmental systems. *ACM Comput. Surv.*, **55**, 66.

Supplementary Information

Physics-informed LSTMs improve streamflow prediction when storage-discharge dynamics are temporally resolved

Alberto Ardid[1,*], David Dempsey[1], Céline Cattoën[2,3], Markus Pahlow[1]

[1] Department of Civil and Environmental Engineering, University of Canterbury, Christchurch, New Zealand

[2] Earth Sciences New Zealand, Christchurch, New Zealand

[3] Te Pūnaha Matatini, University of Auckland, Auckland, New Zealand

Author email addresses

Alberto Ardid: alberto.ardid@canterbury.ac.nz

David Dempsey: david.dempsey@canterbury.ac.nz

Céline Cattoën: celine.cattoengilbert@earthsciences.nz

Markus Pahlow: markus.pahlow@canterbury.ac.nz

Supplementary material status

This supplementary information accompanies a non-peer-reviewed preprint submitted to EarthArXiv. The manuscript has also been submitted to Water Resources Research for peer review.

This file contains

- Supplementary Figures S1-S9
- Supplementary Tables 1-2

Supplementary Information

Physics-informed LSTMs improve streamflow prediction when storage-discharge dynamics are temporally resolved

This file contains:

- Supplementary Figures S1-S9
- Supplementary Tables 1-2

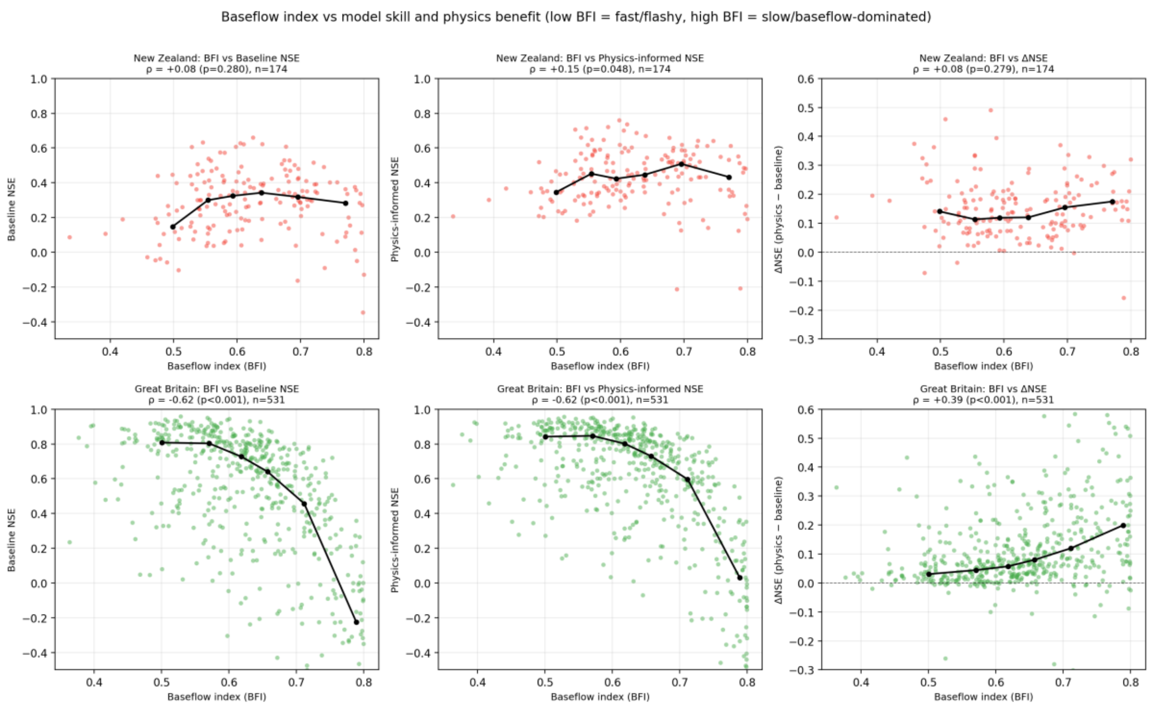

Supplementary Figure S1. Physics benefit in relation to baseline model skill and catchment baseflow signature. Baseflow index (BFI; low = fast, flashy catchments, high = slow, baseflow-dominated catchments) versus baseline NSE (left), physics-informed NSE (centre) and physics benefit (ΔNSE, right) for New Zealand (top, $n = 174$) and Great Britain (bottom, $n = 531$) at hourly resolution. Black lines are binned medians; Spearman ρ and p are annotated in each panel. In Great Britain, ΔNSE increases with BFI ($\rho = +0.39$, $p < 0.001$): gains are larger in baseflow-dominated catchments and smaller in flashy, surface-runoff catchments. In New Zealand, where nearly all catchments improve, the signature relationship is weak.

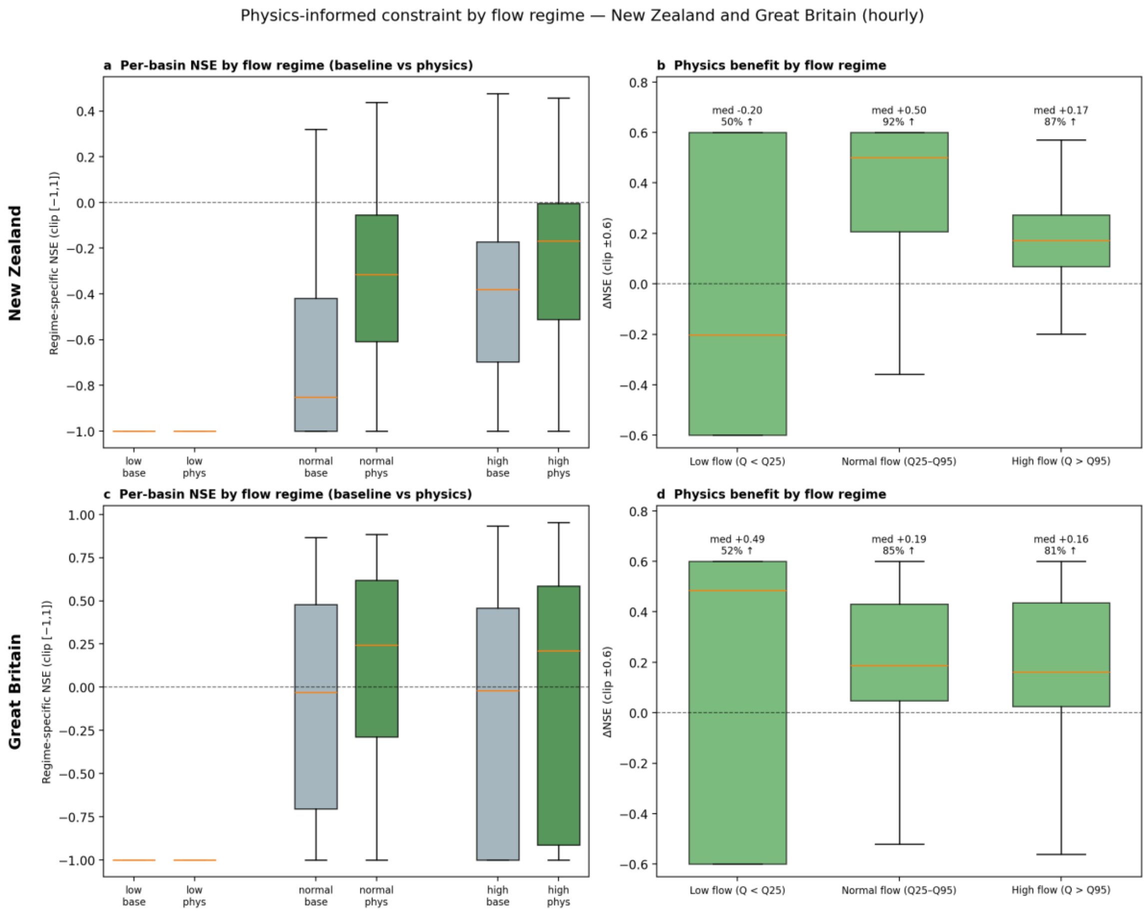

Supplementary Figure S2. Physics-informed constraint by flow regime for New Zealand (top) and Great Britain (bottom) at hourly resolution. (a, c) Per-basin regime-specific NSE for the baseline and physics-informed models in the low- (Q < Q25), normal- (Q25-Q95) and high-flow (Q > Q95) regimes. (b, d) Physics benefit (ΔNSE) by regime; the median ΔNSE and percentage of catchments improved are annotated above each box. Gains concentrate in the normal- and high-flow regimes that dominate hydrograph volume and flood peaks.

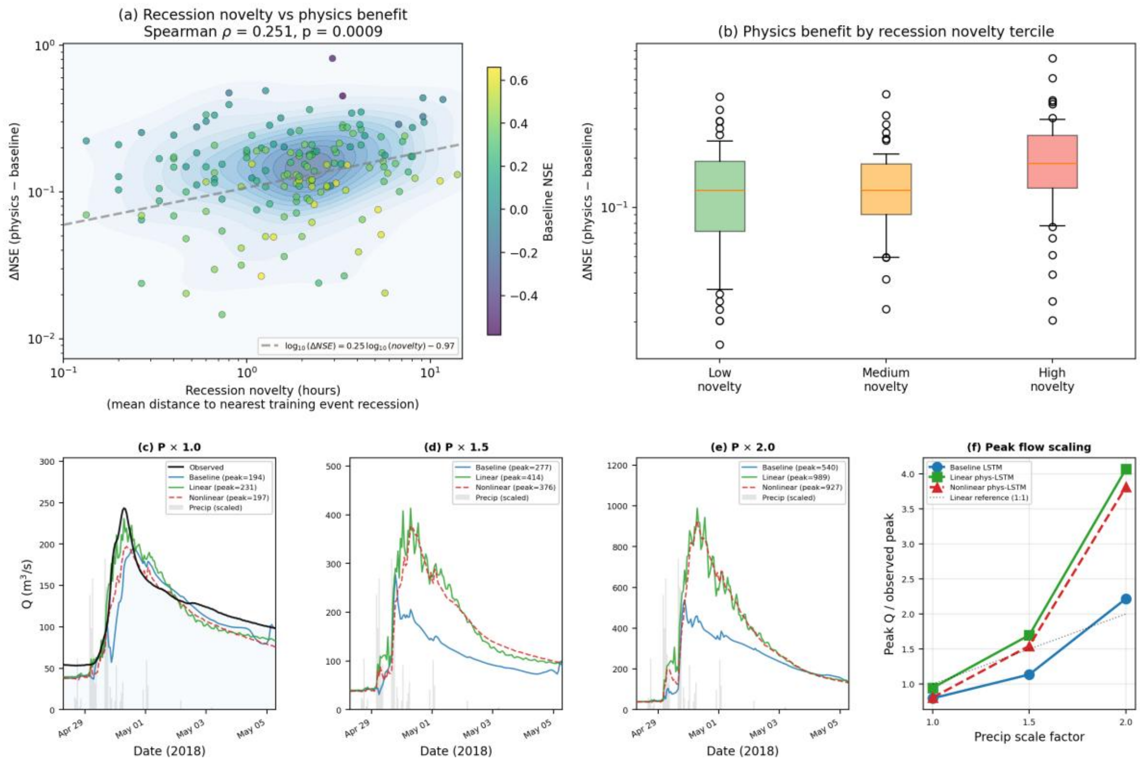

Supplementary Figure S3. Recession novelty and response to synthetic storm scaling (New Zealand, hourly). (a) Physics benefit (ΔNSE) versus recession novelty - the mean distance between test-period flood-recession timescales and the nearest recessions seen during training (Spearman $\rho = 0.251$, $p = 0.0009$). (b) ΔNSE grouped by recession-novelty tercile. (c-e) Observed and modelled hydrographs for an example catchment with precipitation scaled by ×1.0, ×1.5 and ×2.0 while the trained models are held fixed. (f) Peak discharge versus precipitation scale factor: the physics-informed models increase more nearly proportionally, whereas the unconstrained baseline saturates at high forcing.

Supplementary Table 1. Physics benefit by flow regime for New Zealand and Great Britain (hourly). For each regime the median physics benefit (ΔNSE = physics − baseline) and the percentage of catchments improved are shown, with the all-flows summary for reference. Regimes are defined by per-catchment flow quantiles: low (Q < Q25), normal (Q25-Q95) and high (Q > Q95).

Country	Flow regime	N basins	Median ΔNSE	% improved
New Zealand	Low (Q < Q25)	174	-0.203	49.7
New Zealand	Normal (Q25-Q95)	174	+0.500	92.5
New Zealand	High (Q > Q95)	174	+0.172	86.7
New Zealand	All flows	174	+0.106	93.6
Great Britain	Low (Q < Q25)	519	+0.485	52.4
Great Britain	Normal (Q25-Q95)	519	+0.187	84.7
Great Britain	High (Q > Q95)	519	+0.162	81.1
Great Britain	All flows	519	+0.072	91.1

Optimal regularisation weight and catchment area

The optimal regularisation weight λ controls the strength of the physics constraint relative to the data-fitting loss. Supplementary Figure S4 shows the spatial distribution of optimal λ across New Zealand and its relationship with catchment area. Small catchments (< 50 km²) consistently require strong regularisation (λ = 100-1,000), while large catchments (> 1,000 km²) perform best with weak regularisation (λ = 0.01-1.0). The log-linear relationship $\log_{10}(\lambda) = -1.30 \cdot \log_{10}(A) + 4.19$ ($R^2 = 0.47$, Spearman r = −0.73) enables prediction of the optimal λ from catchment area alone, with a median NSE cost of only 0.006 under leave-one-out cross-validation. This is physically intuitive: smaller catchments have fewer independent storm events in the training record, so the LSTM has less data from which to learn recession dynamics and benefits more from the physics prior.

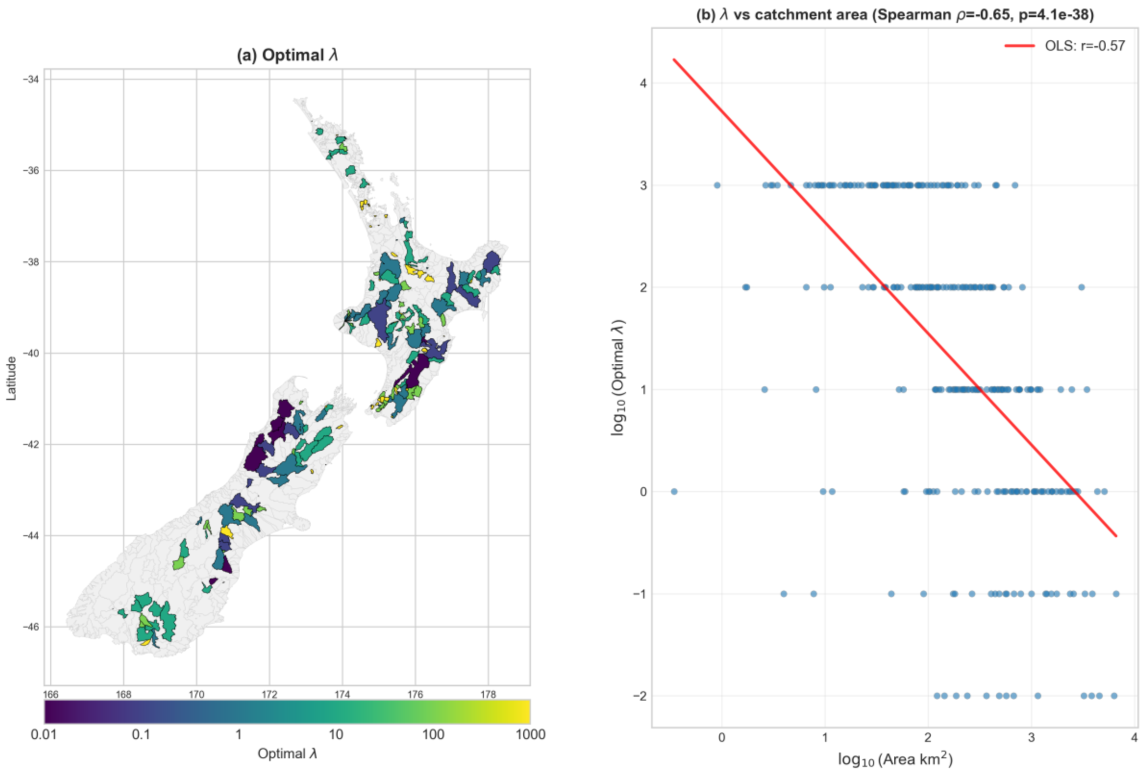

Supplementary Figure S4. Optimal regularisation weight λ versus catchment area for 174 NZ catchments. (a) Map of optimal λ per catchment. (b) Log-linear regression: $\log_{10}(\lambda) = -1.30 \cdot \log_{10}(A) + 4.19$ ($R^2 = 0.47$, Spearman r = −0.73).

Learned recession parameters

Supplementary Figure S5 shows the distribution and spatial pattern of the learned recession coefficient K from the linear reservoir constraint (Q = KS). The median K = 0.087 h^{-1} corresponds to a recession timescale $\tau = 1/K \approx 11.5$ hours, consistent with the rapid response expected of New Zealand's steep, well-drained catchments. The distribution is right-skewed with most values between 0.04 and 0.15 h^{-1}, and shows weak dependence on catchment area (Spearman $\rho = -0.10$), indicating that recession speed is governed more by geology and soil properties than by catchment size. Spatially, faster recession (higher K) tends to occur in steeper, higher-elevation catchments on the west coast.

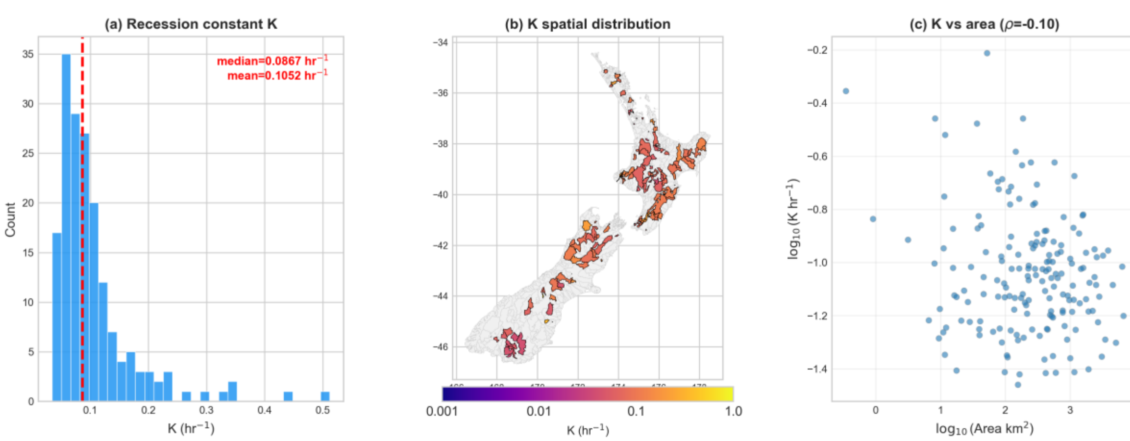

Supplementary Figure S5. Learned recession coefficient K from the linear reservoir constraint. (a) Distribution of K across 174 catchments (median = 0.087 h^{-1}). (b) Spatial distribution of K across New Zealand. (c) K versus catchment area ($\rho = -0.10$).

Performance stratified by catchment properties

Supplementary Figure S6 decomposes the physics benefit (ΔNSE) by catchment properties. The improvement is consistent across all area classes, elevation bands, and stream orders (panels a, b, d), confirming that the physics constraint is broadly beneficial rather than limited to a particular catchment type. However, the largest gains occur where baselines are weakest: ΔNSE shows a negative correlation with baseline NSE (Spearman $\rho = -0.51$, panel c), indicating that the physics prior is most valuable where the unconstrained LSTM struggles. Low-order headwater streams (orders 1-2) show the highest median ΔNSE, consistent with the lambda-area scaling: these small, flashy catchments have the fewest training events and benefit most from the constraint.

Supplementary Table 2 quantifies these trends by area class. The smallest catchments (< 50 km^2) show the largest median improvement (ΔNSE = +0.173) with 100% of basins improved, while the largest catchments (> 1,000 km^2) show a smaller but still substantial improvement (ΔNSE = +0.126), also with 100% improved. The optimal λ decreases systematically from 1,000 for small catchments to 1 for large catchments, spanning three orders of magnitude. Learned K values are consistent across area classes (0.082-0.090 h^{-1}), confirming that the recession coefficient reflects catchment-scale hydrological properties rather than an artefact of the regularisation strength.

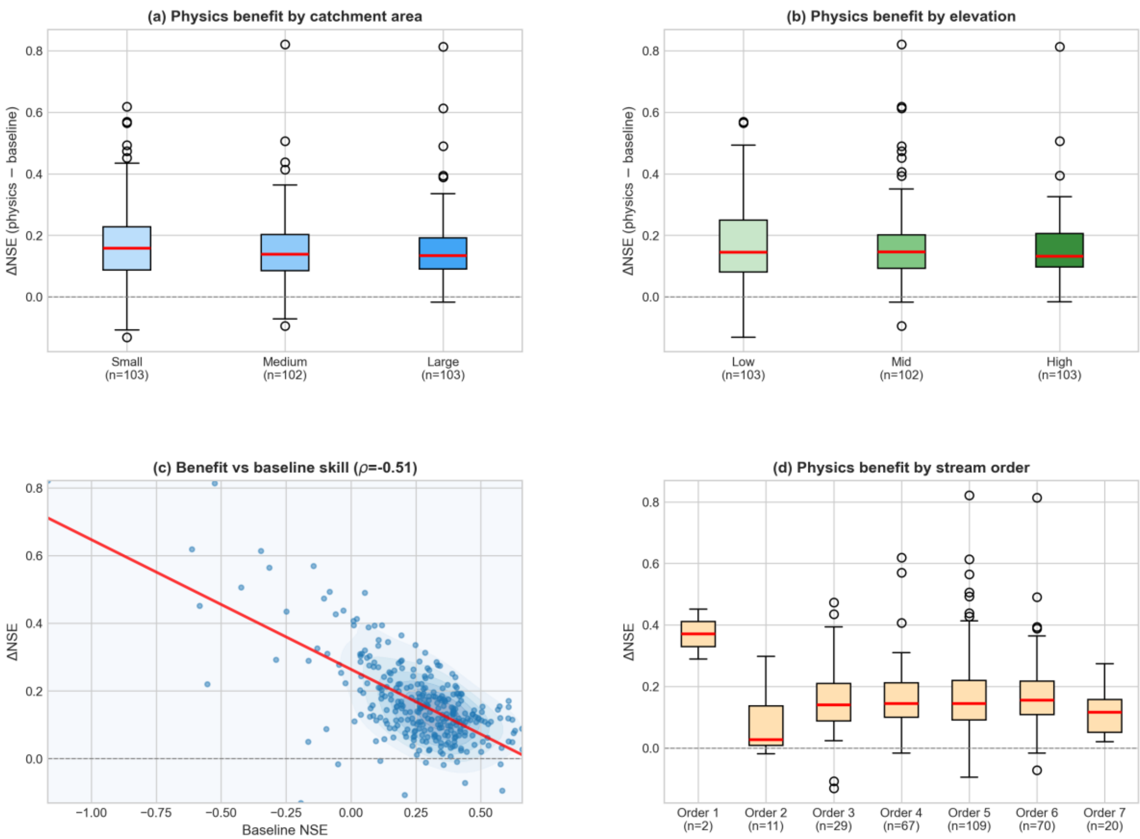

Supplementary Figure S6. Physics benefit stratified by catchment properties. (a) ΔNSE by catchment area class. (b) ΔNSE by elevation class. (c) ΔNSE versus baseline NSE ($\rho = -0.51$). (d) ΔNSE by Strahler stream order.

Supplementary Table 2. Summary statistics for the New Zealand hourly experiment by catchment area class. Catchments are divided into four area classes spanning 0.3 to 6,643 km^2.

Area class (km^2)	**N**	**Med. baseline NSE**	**Med. physics NSE**	**Med. ΔNSE**	**% improved**	**Med. K (h^{-1})**	**Med. λ**
< 50	34	0.180	0.344	+0.173	100.0	0.083	1,000

50-200	42	0.213	0.381	+0.153	97.6	0.082	100
200-1,000	64	0.342	0.484	+0.149	98.4	0.090	10
> 1,000	34	0.415	0.580	+0.126	100.0	0.082	1

Linear versus nonlinear reservoir

Supplementary Figure S7 compares the linear (Q = KS) and nonlinear (Q = KS^n) reservoir formulations. The scatter plot (panel a) shows that the two models produce nearly identical performance, with the nonlinear model marginally better in 54% of catchments. The distribution of NSE differences (panel b) is tightly centred near zero (median = +0.002), confirming that the nonlinear extension provides minimal additional benefit. The learned nonlinear exponent clusters near n = 1.79, suggesting mildly convex storage-discharge behaviour consistent with theoretical predictions for heterogeneous catchments. The near-equivalence of the two formulations supports the use of the simpler linear reservoir as the primary constraint.

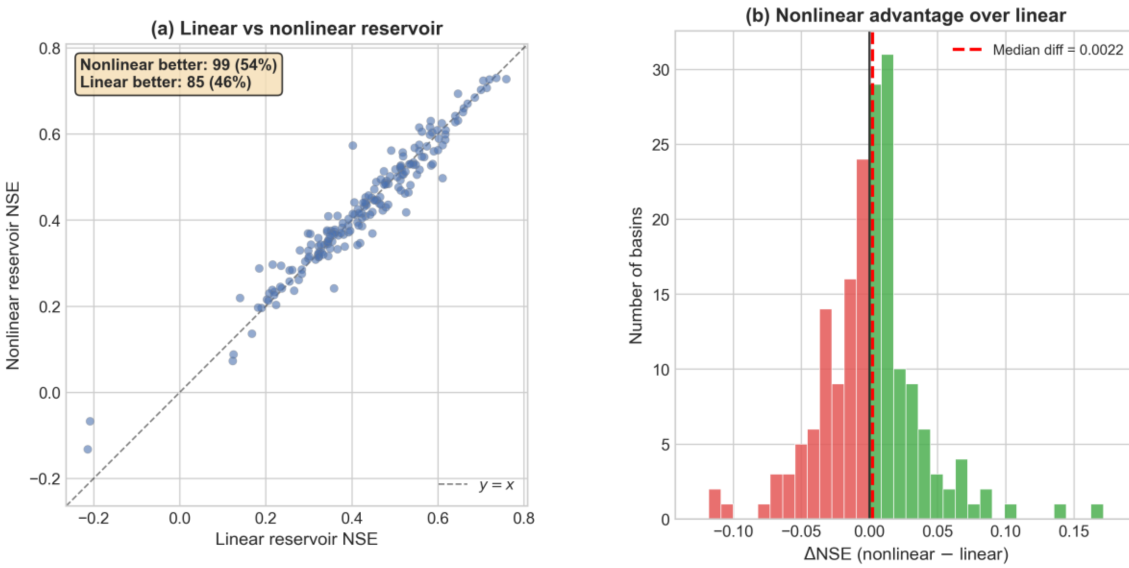

Supplementary Figure S7. Linear versus nonlinear reservoir comparison. (a) Scatter of linear versus nonlinear NSE. The nonlinear model is marginally better in 54% of catchments. (b) Distribution of NSE difference (median = +0.002).

Resolution comparison: hourly versus daily

Supplementary Figure S8 directly compares the effect of the physics constraint at hourly and daily resolution for 173 New Zealand catchments common to both experiments. At hourly resolution (orange), the ΔNSE distribution is shifted strongly positive (median = +0.14, 99% improved). At daily resolution (green), the distribution shifts negative (median = −0.15, only 14% improved). The per-basin scatter (panel b) shows that 148 catchments improve at hourly but not daily resolution, while zero catchments show the reverse pattern. Only 24 catchments improve at both resolutions. This paired comparison, same basins, same architecture, same constraint, different temporal aggregation, isolates resolution as the critical factor.

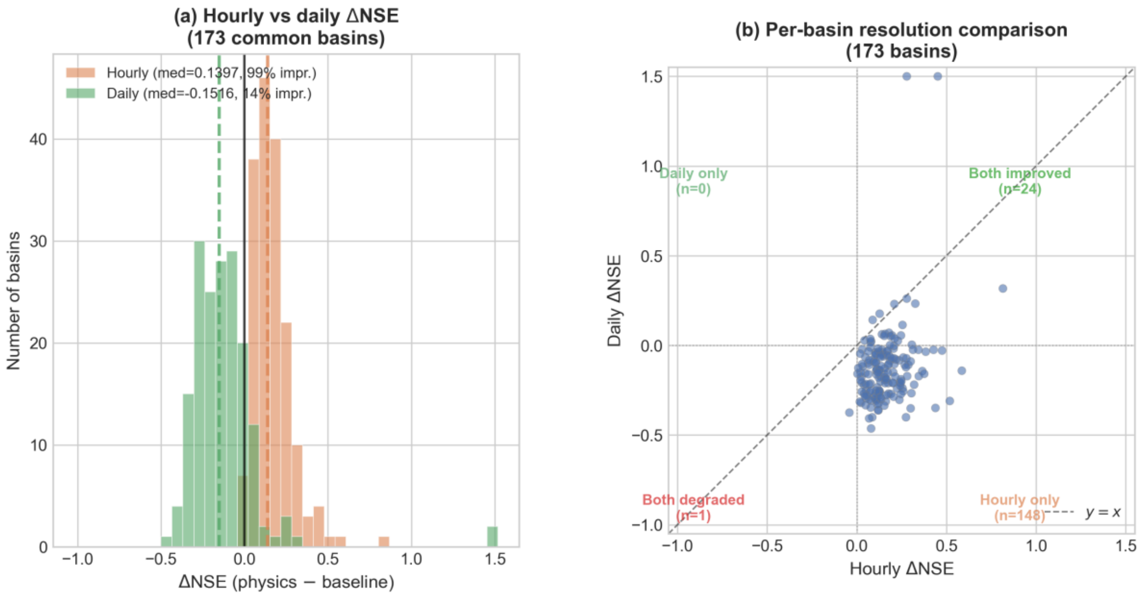

Supplementary Figure S8. Resolution comparison for 173 New Zealand catchments. (a) Distribution of ΔNSE at hourly (orange, 99% improved) and daily (green, 14% improved) resolution. (b) Per-basin scatter of hourly versus daily ΔNSE.

Comprehensive parameter and benefit analysis

Supplementary Figure S9 provides a comprehensive six-panel view of the physics benefit and learned parameters. The negative correlation between ΔNSE and baseline NSE ($\rho = -0.55$, panel a) confirms that the constraint helps most where the unconstrained model is weakest. The K distribution (panel b) and optimal λ distribution (panel c) summarise the learned physics parameters across all catchments; the median $\lambda = 10$ reflects the typical regularisation strength. K shows weak dependence on catchment area (panel d, $\rho = -0.10$), indicating that the learned recession coefficient captures intrinsic catchment properties. The physics benefit is consistent across geological classes (panel e), with no geology showing systematically different improvement. Similarly, ΔNSE shows minimal dependence on catchment area (panel f, $\rho = -0.09$), confirming that the physics constraint benefits catchments of all sizes.

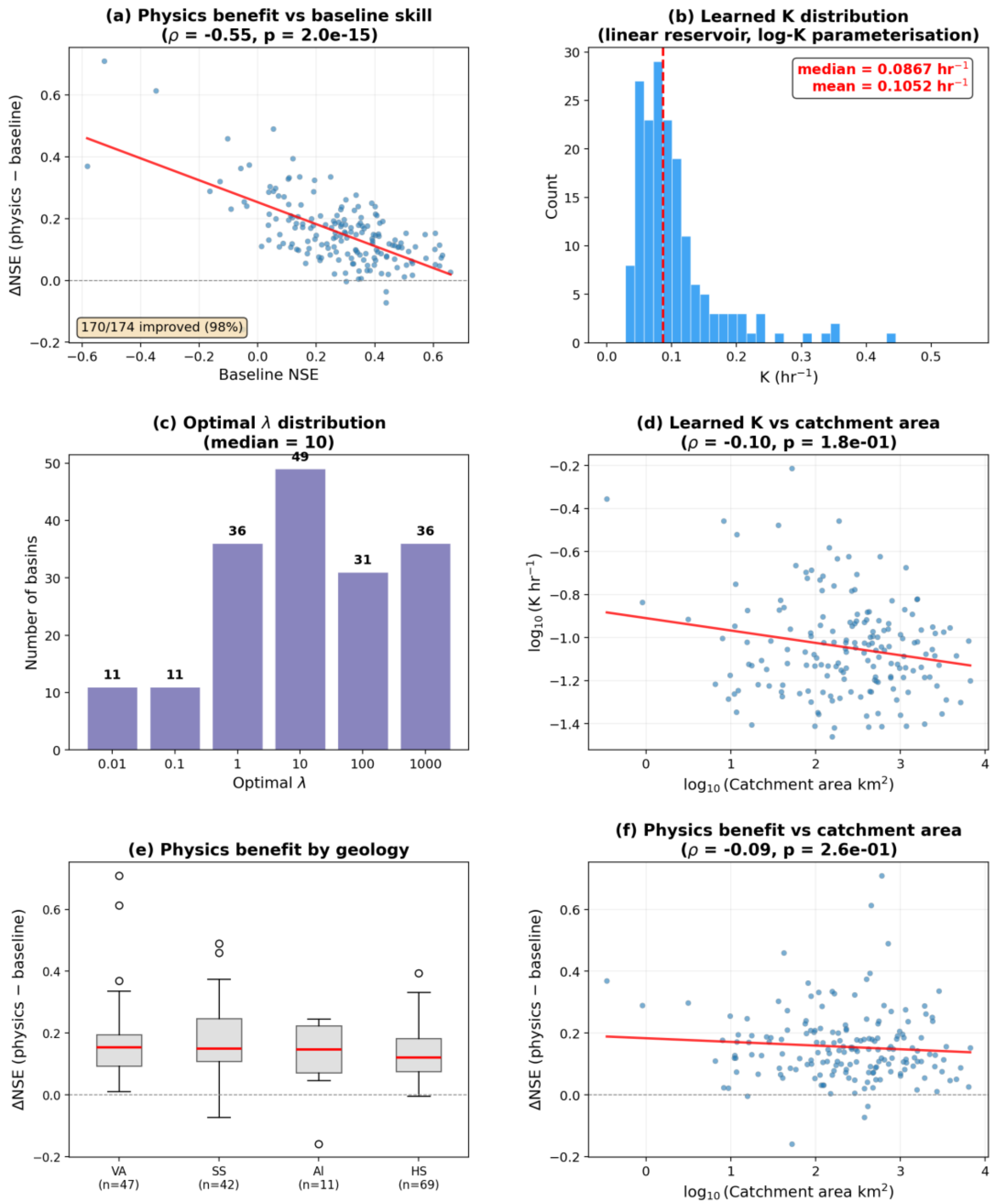

Supplementary Figure S9. Physics benefit and learned parameters. (a) ΔNSE versus baseline NSE ($\rho = -0.55$). (b) Learned K distribution. (c) Optimal λ distribution. (d) K versus catchment area. (e) ΔNSE by geology. (f) ΔNSE versus catchment area.